Polycrystalline SnO_2 Nanotubes Prepared via Infiltration Casting of Nanocrystallites and Their Electrochemical Application

Yong Wang,[†] Jim Yang Lee,[†,‡] and Hua Chun Zeng*[,‡]

Singapore−MIT Alliance, National University of Singapore, 4 Engineering Drive 3, Singapore 117576, and Department of Chemical and Biomolecular Engineering, Faculty of Engineering, National University of Singapore, 10 Kent Ridge Crescent, Singapore 119260

Received April 5, 2005. Revised Manuscript Received May 30, 2005

In this work we demonstrated that uniform polycrystalline SnO_2 nanotubes, in either array or free-standing form, can be fabricated by an infiltration technique using SnO_2 nanoparticles as starting building units. With this method, the diameter, length, thickness, and texture of the nanotubes can be further controlled. The tubular SnO_2 shows a significant improvement of electrochemical performance over the unorganized nanoparticles. The specific capacity of the Sn-based nanotube electrode was 525 mAh/g after 80 cycles. In principle, the tubular structure of active component can also be extended to other metal oxides and Li−metal alloy systems. In view of their unique features, the prepared SnO_2 nanotubes may also find interesting applications in other fields such as gas sensing.

Introduction

Over the past decade, there has been a strong research interest in 1D nanomaterials, owing to their novel physicochemical properties and potential applications in many new technologies.[1−15] Past synthetic advancement has allowed one to prepare this class of materials into various morphological forms such as nanotubes, nanorods, nanoribbons, and nanowires.[1,2,5] Among different synthetic strategies, in particular, anodic aluminum oxide (AAO) and polycarbonate (PC) membrane-template methods have been widely used in fabrication of tubular 1D nanomaterials.[1,2c,7,14,15] For example, a wide range of transition-metal oxide nanotubes (such as TiO_2, WO_3, and ZnO)[1] has been prepared with sol−gel approaches in which metal-containing sols were introduced to the 1D nanoporous channels of AAO membranes, followed by thermal calcinations at elevated temperatures and subsequent removal of alumina templates. Besides the metal oxides, furthermore, polyelectrolyte nanotubes and polyelectrolyte−nanoparticle hybrid nanotubes have also been fabricated with the assistance of PC membrane templates via layer-by-layer coating routes.[2c] Recent progress in this area shows that the above templating strategies can also be coupled with more established processing methods such as electroless plating, chemical vapor deposition, polymerization, and layer-by-layer ionic coating in achieving a wide variety of functional materials with tubular morphology.[15] Very recently, gold (or silver, 14 ± 2 nm in diameter) colloidal solutions have been introduced to silanized AAO templates by vacuum suction, accompanied by spontaneous room-temperature coalescence of the bound metal nanoparticles.[7] This novel process indicates for the first time that tubular nanostructures can also be constructed form 0D building units (i.e., formation of metallic nanoparticle nanotubes).

In the present work, we will use the fabrication of polycrystalline SnO_2 nanotubes as an example to demonstrate that, in addition to the above metallic nanoparticle nanotubes, metal oxide nanotubes can also be prepared with their primitive 0D nanoparticles (6−15 nm in diameter) with assistance of AAO templating. The present synthetic approach involves an infiltration casting of premade colloidal SnO_2 nanoparticles into 1D channels of AAO membranes, generation of chemical binding among nanoparticles via thermal treatment, and removal of AAO templates in NaOH solutions.

In addition to the above synthetic investigation, a secondary objective in the present work is to examine the structural

* To whom correspondence should be addressed. E-mail: chezhc@nus.edu.sg.

[†] Singapore−MIT Alliance, Nation University of Singapore.

[‡] Department of Chemical and Biomolecular Engineering, National University of Singapore.

(1) (a) Lakshmi, B. B.; Dorhout, P. K.; Martin, C. R. *Chem. Mater.* **1997**, *9*, 857. (b) Yu, S. F.; Li, N. C.; Wharton, J.; Martin, C. *Nano Lett.* **2003**, *3*, 815. (c) Mitchell, D. T.; Lee, S. B.; Trofin, L.; Li, N. C.; Nevanen, T. K.; Soderlund, H.; Martin, C. R. *J. Am. Chem. Soc.* **2002**, *124*, 11864. (d) Sides, C. R.; Li, N. C.; Patrissi, C. J.; Scrosati, B.; Martin, C. R. *Mater. Res. Soc. Bull.* **2002**, *27*, 604.

(2) (a) Caruso, R. A. *Angew. Chem., Int. Ed.* **2004**, *43*, 2746. (b) Caruso, R. A. Schattka, J. H.; Greiner, A. *Adv. Mater.* **2001**, *13*, 1577. (c) Liang, Z.; Susha, A. S.; Yu, A.; Caruso, F. *Adv. Mater.* **2003**, *15*, 1849.

(3) (a) Zheng, M.; Li, G.; Zhang, X.; Huang, S.; Lei, Y.; Zhang, L. *Chem. Mater.* **2001**, *13*, 3859. (b) Steinhart, M.; Wendorff, J. H.; Greiner, A.; Wehrspohn, R. B.; Nielsch, K.; Schilling, J.; Choi, J.; Gösele, U. *Science* **2002**, *296*, 1997.

(4) Dai, Z. R.; Gole, J. L.; Stout, J. D.; Wang, Z. L. *J. Phys. Chem. B* **2002**, *106*, 1274.

(5) Rao, C. N. R.; Nath, M. *Dalton Trans.* **2003**, 1 and the references therein.

(6) Tenne, R. *Angew. Chem., Int. Ed.* **2003**, *42*, 5124.

(7) Lahav, M.; Sehayek, T.; Vaskevich, A.; Rubinstein, I. *Angew. Chem., Int. Ed.* **2003**, *42*, 5576.

(8) Li, F.; He, J.; Zhou, W. L.; Wiley, J. B. *J. Am. Chem. Soc.* **2003**, *125*, 16166.

(9) Liu, Y.; Dong, J.; Liu, M. *Adv. Mater.* **2004**, *16*, 353.

(10) Liu, B.; Zeng, H. C. *J. Phys. Chem. B* **2004**, *108*, 5867.

(11) Vayssieres, L.; Graetzel, M. *Angew. Chem., Int. Ed.* **2004**, *43*, 3666.

(12) Yang, H. G.; Zeng, H. C. *Angew. Chem., Int. Ed.* **2004**, *43*, 5206.

(13) Lu, Q.; Gao, F.; Komarneni, S.; Mallouk, T. E. *J. Am. Chem. Soc.* **2004**, *126*, 8650.

(14) Chen, J.; Tao, Z. L.; Li, S. L. *J. Am. Chem. Soc.* **2004**, *126*, 3060.

(15) Steinhart, M.; Wehrspohn, R. B.; Gösele, U.; Wendorff, J. H. *Angew. Chem., Int. Ed.* **2004**, *43*, 1334.

10.1021/cm050724f CCC: $30.25
Published on Web 06/29/2005

effect of the resultant nanotubes. The material SnO_2 chosen herein has been proposed as a promising substituent for commercial graphite,[16−21] owing to its high storage capacity (theoretical value: ~790 mAh/g (SnO_2); vs 372 mAh/g of the graphite).[22−29] Nonetheless, the main hindrance against the commercial use of SnO_2 has been known to be the severe volume expansion and contraction during the alloying−dealloying cycles with Li^+ ions and associated charge-transfer process.[30,31] Apart from the pulverization, another critical problem for tin-based anodes is agglomeration of primitive particles, which drastically reduces the total entrance/exit sites available for Li^+ ions (i.e., reduction in surface-to-volume ratio) and creates even more severe mechanical stresses in the surface region of a particulate aggregate. One might consider that a pre-organization of 0D SnO_2 nanoparticles into tubular configurations may partially circumvent the above technological dilemmas. Quite encouragingly, our preliminary material evaluations indeed indicate that improved electrochemical performance and cyclability for lithium ion charge and discharge can be attained using the resultant polycrystalline tubular precursors. This improvement can be attributed to their tubular organizing structure and interconnectivity among the particles generated at high-temperatures.

Experimental Section

A low concentration of SnO_2 (3 wt %) suspension was prepared by adding deionized water to an as-received colloidal SnO_2 aqueous suspension (15 wt %, Nyacol Nano Technologies, Inc., SN-15; SnO_2 particle sizes in the range of 10−15 nm, negatively charged). This colloidal suspension was then sonicated for 20 min to diminish possible colloidal aggregation. The porous anodized alumina membranes (Whatman, Anodisc, $\phi = 200$ nm) were immersed in water for 30 min under vacuum to remove the air bubbles within the pores and then dried before their use for SnO_2 nanotube preparation.

The SnO_2 nanotubes were fabricated by colloidal infiltration into the membrane channels for a number of cycles. In each casting experiment, the above pretreated alumina membrane was placed on a piece of filter paper. The prepared dilute SnO_2 colloidal suspension (0.1−0.4 mL; 3 wt %) was then infiltrated into the membrane under vacuum. The upper surface of membrane was then polished gently by sand paper (2500 grid). The same procedure was repeated for 1−8 times in order to attain a desired thickness for the nanotube walls. After dried in air, the SnO_2-encapsulated alumina membrane was calcined in normal laboratory air at 650 °C for 10 h. The alumina template was removed in a NaOH aqueous solution (1.0 M for 10 h or 6.0 M for 30 min). The SnO_2 nanotube product was washed with copious deionized water, followed by centrifuging and drying (5000 rpm; 130 °C in a vacuum oven for 3 h). The centrifugation employed here did not cause additional fragmenting impact on the as-prepared SnO_2 nanotubes.

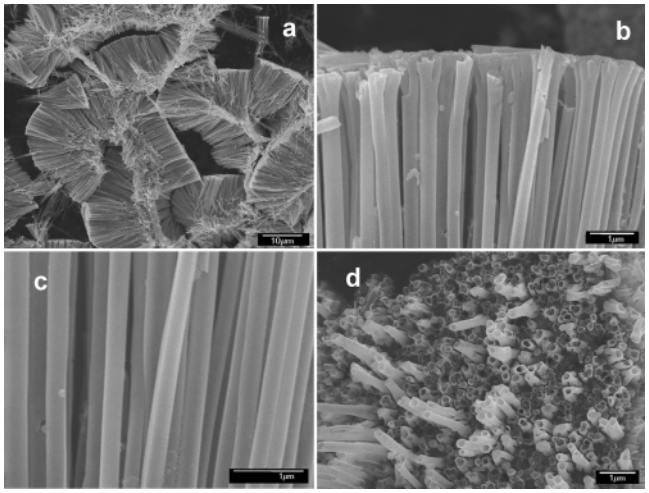

Figure 1. FESEM images of the SnO_2 nanotubes prepared by infiltration after 8 cycles: (a) Large assemblies of as-prepared nanotubes. (b) Side view of top section. (c) Side view of body section. (d) Top view of nanotubes.

The room-temperature electrode activities were measured by a Maccor-Series-2000 battery tester (with anode Li^+/Li).[16] The working electrode consisted of 60 wt % of the active component (SnO_2; ~500 $\mu g/cm^2$), 30 wt % of conductive agent (carbon black, Super-P), and 10 wt % of binder (poly(vinylidene difluoride), PVDF, Aldrich). All cells were tested at the constant current density of 0.05 mA/cm^2 (C rate = 0.125 h^{-1}) and were charged (Li^+ insertion) and discharged (Li^+ extraction) between fixed voltage limits (5 mV to 2 V). The as-obtained and used SnO_2 materials were characterized by field-emission scanning electron microscopy (FESEM, JEOL JSM-6700F), transmission electron microscopy (TEM), selected area electron diffraction (TEM/SAED, JEOL JEM-2010F), high-resolution TEM (HRTEM/SAED, Philips FEG-CM300), and powder X-ray diffraction (XRD, Shimadzu XRD-6000, Cu Kα radiation).

Results and Discussion

Figure 1 reports the product morphology of the SnO_2 nanotubes prepared in this work. After removal of alumina templates, the nanotube products are generally in the form of bundles (Figure 1a). The nanotubes are very uniform with constant diameters in the range of ~180−230 nm (parts b and c of Figure 1), in accordance to the denoted pore size (~200 nm) of the AAO membranes. A top view of the obtained nanotubes is displayed in Figure 1d. The tubular nanostructures with opening are well aligned, and the cross section of these nanotubes is indeed circular (Supporting Information 1). Analysis with energy-dispersive X-ray

(16) Wang, Y.; Lee, J. Y.; Chen, B. H. *J. Electrochem. Soc.* **2004**, *151*, A563.
(17) Shimoda, H.; Gao, B.; Tang, X. P.; Kleinhammes, A.; Fleming, L.; Wu, Y.; Zhou, O. *Phys. Rev. Lett.* **2002**, *88*, 015502.
(18) Idota, Y.; Kubota, T.; Matsufuji, A.; Maekawa, Y.; Miyasaka, T. *Science* **1997**, *276*, 1395.
(19) Winter, M.; Besenhard, J. O.; Spahr, M.; Novak, P. *Adv. Mater*. **1998**, *10*, 725.
(20) Courtney, I. A.; Mckinno, W. R.; Dahn, J. R. *J. Electrochem. Soc*. **1999**, *146*, 59.
(21) Li, N.; Martin, C. R.; Scrosati, B. *Electrochem. Solid-State Lett*. **2000**, *3*, 316.
(22) Li, H.; Wang, Q.; Shi, L.; Chen, L.; Huang, X. *Chem. Mater*. **2002**, *14*, 103.
(23) Behm, M.; Irvine, J. T. S. *Electrochim. Acta* **2002**, *47*, 1727.
(24) Limthongkul, P.; Wang, H.; Jud, E.; Chiang, Y. M. *J. Electrochem. Soc.* **2002**, *149*, A1237.
(25) Yoshio, M.; Wang, H.; Fukuda, K. *Angew. Chem., Int. Ed.* **2003**, *42*, 4203.
(26) Lee, K. T.; Jung, Y. S.; Oh, S. M. *J. Am. Chem. Soc.* **2003**, *125*, 5652.
(27) Yan, H. W.; Sokolov, S.; Lytle, J. C.; Stein, A.; Zhang, F.; Smyrl, W. H. *J. Electrochem. Soc.* **2003**, *150*, A1102.
(28) Fan, J.; Wang, T.; Yu, C.; Tu, B.; Jiang, Z.; Zhao, D. *Adv. Mater*. **2004**, *16*, 1432.
(29) Wang, Y.; Lee, J. Y. *J. Phys. Chem. B* **2004**, *108*, 17832.
(30) Winter, M.; Besenhard, J. O. *Electrochim. Acta* **1999**, *45*, 31.
(31) Tarascon, J. M.; Armand, M. *Nature* **2001**, *414*, 359.

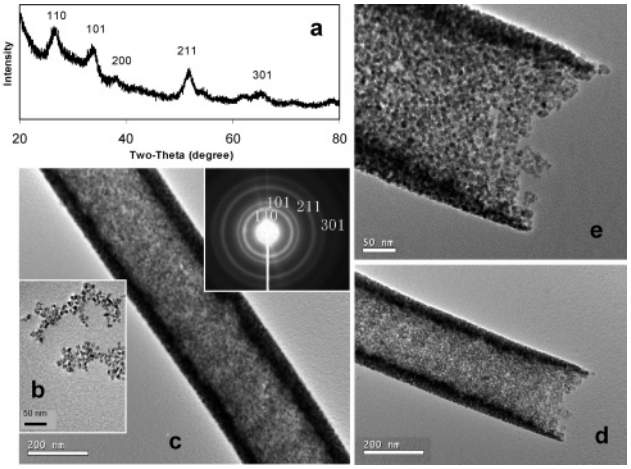

Figure 2. (a) The XRD pattern of SnO_2 nanotubes prepared after 8 cycles of infiltration. (b) TEM image of the primitive SnO_2 nanoparticles. (c) TEM images of an individual SnO_2 nanotube prepared after 8 cycles of infiltration (inset is its corresponding SAED pattern). (d and e) The open end of the same nanotube in (c) at different magnifications.

spectroscopy reveals that the atomic ratio of Sn:O is equal to 1:2, confirming the stoichiometry of the products. The crystallographic information is further established with powder XRD. As shown in a XRD pattern of Figure 2a, all the diffraction peaks can be indexed to the rutilelike SnO_2 with tetragonal lattice constants $a_0 = 4.74$ Å and $c_0 = 3.19$ Å (JCPDS 41−1445).[4,10]

The as-received commercial SnO_2 nanoparticles are examined with TEM in Figure 2b. The particles, which were used as the starting building units for SnO_2 nanotubes, are slightly agglomerated with sizes in the range of ∼6−15 nm (denoted range: 10−15 nm). The TEM investigation (Figures 2 and 3) indicates that there was no appreciable particle growth after the thermal treatment at 650 °C, although the crystallinity was improved. The rutile phase of SnO_2 is also reflected in the SAED pattern, in agreement with the XRD result. The nanocrystalline wall structure is further detailed with HRTEM technique. As reported in parts a and b of Figure 3, the nanotube walls are indeed polycrystalline, comprising numerous nanocrystallites with the sizes of ∼6−15 nm, similar to the starting sizes of Figure 2a. The thickness of the tube walls can be controlled in the range of about 10−25 nm, depending on the number of infiltration adopted (Supporting Information 2). Interestingly, even with a higher infiltration number, the porous nature of the nanotube walls is still maintained (parts a and b of Figure 3). It is believed that this additional intra-wall space not only can provide extra routes for Li^+ transport/insertion but also can enhance dimensional susceptibility for nanotubes to undergo large volume changes incurring during charging−discharging cycles. The above observations were also verified with FESEM investigation, similar morphological conclusions can also be drawn (Supporting Information 1).

In addition to the control of wall thickness, the length of SnO_2 nanotubes can also be tailored. By use of a higher concentration NaOH solution (6.0 M) to remove the alumina template, followed by 5 min of sonication, the as-prepared nanotubes can be shortened, compared to the use of 1.0 M NaOH. The short SnO_2 nanotubes shown in Figure 3c have more openings, noting that the diffusion path for Li^+ ions

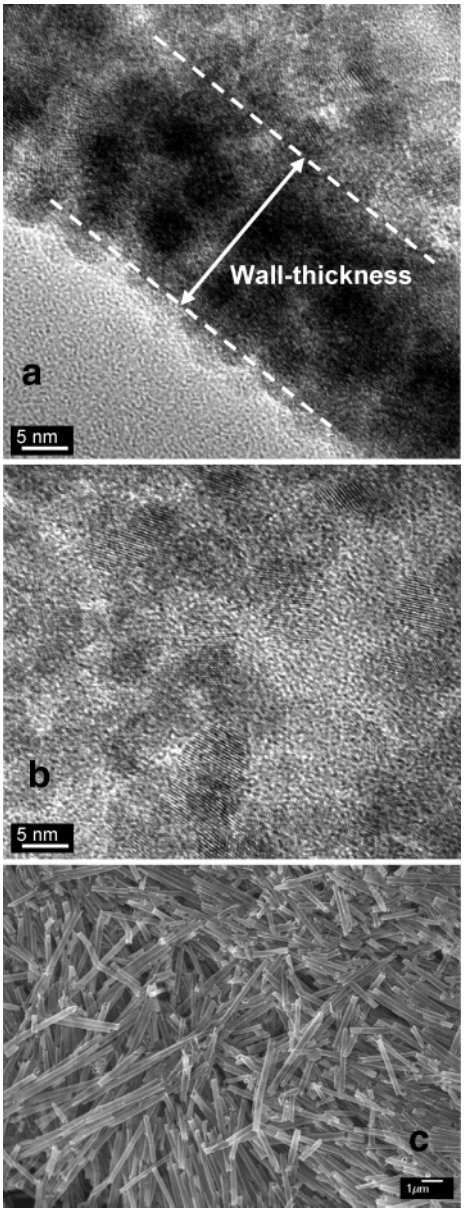

Figure 3. HRTEM images of a tin oxide nanotube by infiltration after 8 cycles: (a) edge part for measuring wall-thickness and (b) middle section of nanotube. A FESEM image (c) of the shortened tin oxide nanotubes after etching (with 6.0 M NaOH).

into internal surfaces has been significantly decreased for the shortened nanotubes.[17] Quite surprisingly, the bundlelike array observed in the long nanotubes (Figure 1) can be avoided for the short nanotubes; these nonaggregated nanotubes may allow a more intimate contact with blending chemicals and prevent the intertube agglomeration.

In view of the good dispersity obtained, the above prepared polycrystalline SnO_2 nanotubes may be useful in overcoming some of the current technical difficulties of tin-oxide-based anode materials in Li^+ ion secondary battery applications. As depicted in Figure 4a, mechanical stresses, which inherit over the volumetric variation, are the main cause for inducing electrode pulverization and resulting in poor cycling performance.[19−21] This technical difficulty has been circumvented partially with matrix isolation methods, in which tin particles were limited to expand and contract within confined spaces of composite matrixes.[26,30] To further improve the performance of this class of materials, we proposed a

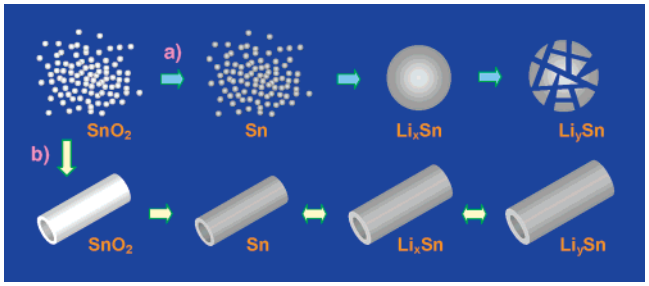

Figure 4. Schematic illustrations of SnO_2 in two different anodic material fabrications: (a) When primitive SnO_2 nanoparticles are used without preorganization, aggregations of resultant Sn (or Li_xSn) and pulverization of Li_ySn (assuming $y \gg x$) occur upon intercalation and deintercalation of lithium ions. (b) When nanocrystallites of SnO_2 are organized into a tubular configuration, concentric expansion and contraction could be expected upon lithium charging and discharging.

working scheme as illustrated in Figure 4b. It is anticipated that the concentric expansion and contraction might be attainable from tubular organizations of SnO_2 nanocrystallites when electrochemical reactions take place. In addition to keeping its structural integrity, a tubular structure also has a large interior space to accommodate tensional stresses imposed. Furthermore, the open ends and flexible thin wall structures would allow a more efficient Li^+ ion diffusion from both exterior and interior surfaces, resulting in a more symmetric volume transformation and a larger charge storage.

To test the above working scheme, the short SnO_2 nanotubes, together with conductive carbon black and a binder (polyvinylidene difluoride, PVDF) were selected in our electrochemical tests. The batteries were charged and discharged at a low constant current density of 0.05 mA/cm^2 with a cutoff voltage window of 5 mV to 2 V. The first charge−discharge curves of the prepared SnO_2 nanotubes and as-received nanoparticles are plotted respectively in Figure 5a. The plateau at around 0.8 or 1.0 V scan could be identified as the reduction of SnO_2 (to metallic Sn and Li_2O) and the formation of a solid-electrolyte interface (SEI) layer on the nascent Sn surface.[20,21,30,32] After the formation of Li_x-Sn, Li^+ insertion and extraction reactions would proceed reversibly (Figure 4b).

The cyclabilities of the nanotubes and their primitive nanoparticles are compared in Figure 5b. The first specific capacity of the primitive (i.e., unorganized) SnO_2 is at ~676 mAh/g, and this value is dropped to 65 mAh/g after 80 cycles, corresponding to 9.6% of the initial value. The fast capacity fading with SnO_2 nanoparticles has been a well-known phenomenon.[19,26,28,30] Although nanoscale particles can result in a better cycling performance than micrometer-sized particles by causing a more homogeneous volume change and reducing absolute volume change,[19,30] nanoparticles would nonetheless aggregate into larger particles, and the resulting large particles could be easily pulverized owing to an asymmetrical volume change (Figure 4a).[19−22,26,28,32] Compared to the unorganized SnO_2 nanoparticles, a great difference can be noted for the working electrodes prepared with our SnO_2 nanotubes. The initial capacity of SnO_2

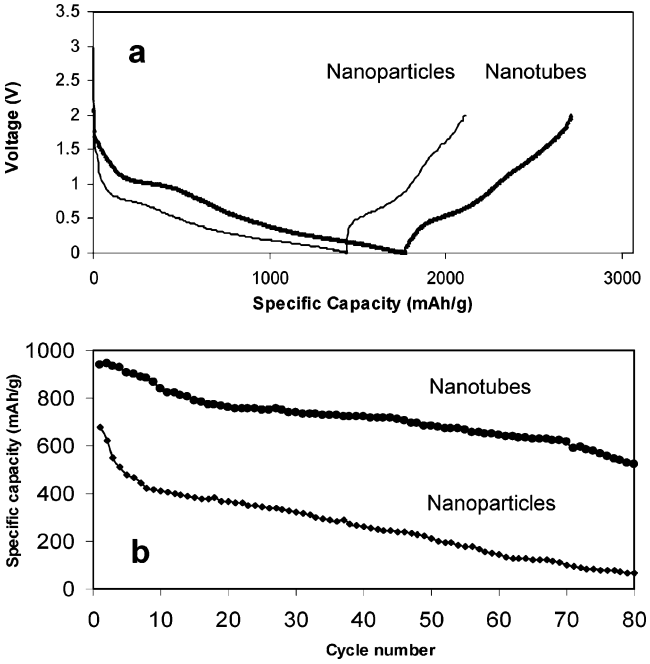

Figure 5. (a) The first cycle charge and discharge of SnO_2 nanotube electrodes (5 mV to 2 V, 0.05 mA/cm^2; voltage vs Li^+/Li). (b) Cyclabilities of SnO_2 nanotube electrodes and SnO_2 nanoparticle electrodes (5 mV to 2 V, 0.05 mA/cm^2; voltage versus Li^+/Li).

nanotubes is at ~940 mAh/g; this value can be retained as big as 525 mAh/g after 80 cycles, which corresponds to 55.8% of the initial specific capacity. This retaining rate (55.8%) is about 6 times as high as that of the nanoparticles (9.6%). It should be mentioned that the specific capacity (525 mAh/g) of SnO_2 nanotubes after 80 cycles was not only higher than that of the nanoparticles (67 mAh/g) but also substantially greater than the theoretical value (372 mAh/g) of commercial graphite anodes.

To verify the operating model proposed in Figure 4b, TEM investigation on the electrode sample after 80 cycles was further carried out. This TEM examination indicates that cylindrical Sn-based structures with almost same dimension as those of Figure 3c were well preserved after so many lithiation−delithiation cycles (230−250 nm in diameter; Supporting Information 3). According to TEM image contrasts, the interior of nanotube seems to become less hollow, which is probably due to the inclusion of the carbon black and binder PVDF during the electrode preparation. This observation supports our postulation in Figure 4b. In addition to the concentric buffer mechanism, axial elongation and restoration of nanotubes should also be recognized.

Therefore, the above improved cycling performance can be attributed to the following points: (1) the central cavities (~150−180 nm in diameter) of the nanotubes can provide a sufficient space to sustain the volume change (~200−260%) associated with Li^+ insertion and extraction.[28,30] Furthermore, the intercrystallite space generated within the nanotube walls (~10−25 nm in wall thickness) has a similar effect to relieve mechanical stresses. Therefore, the electrode "pulverization" could be suppressed by the two-tiered void spaces. (2) Li^+ ions have multiple entrances/exits during the charging−discharging which include porous external and

(32) Zhu, J.; Lu, Z.; Aruna, S. T.; Aurbach, D.; Gedanken, A. *Chem. Mater.* **2000**, *12*, 2557.

internal surfaces as well as tube openings.[17,33,34] The faster Li^+ ion transport in the open-ended tubules can also ensure a more uniform volume change occurring simultaneously across the entire nanotubes. In contrast, only the external surface is available for agglomerated particles. In such a case, Li^+ ions can only insert from the external surface, leading to inhomogeneous volume change between the surface and solid core. (3) Although small SnO_2 nanoparticles may possess high surface area, they are mobile and tend to aggregate if there is no matrix confinement.[22,26,28,32] In comparison, tubular materials are 1D and they will be less movable. Because of their curved surfaces, furthermore, the direct contact among nanotubes can be minimized and less agglomeration is expected. Geometrically, therefore, the tubular organization is even better than 2D filmlike aggregates.[19,30] It is important to recognize that the present porous and polycrystalline SnO_2 nanotubes are in fact more desirable than smooth and continuous single-crystal SnO_2 nanotubes concerning the Li^+ intercalation and deintercalation, because of lacking buffer space in the latter counterparts.

The specific capacity of SnO_2 nanotubes in the first cycle is approximately ~940 mAh/g, which is higher than the theoretical value of SnO_2 (~790 mAh/g) based on the stoichiometry of $Li_{4.4}Sn$.[30] The observed high capacity could last for a few cycles, which is similar to a previous observation using SnO_2 nanorods.[29] This observation can be attributed to background reactions due to the high starting voltage (2 V) used in the present work, compared to the 1-V high-potential limit commonly employed.[35]

Conclusions

In summary, uniform polycrystalline SnO_2 nanotubes (in either array or free-standing form) can be fabricated with an infiltration technique using nanoscale building units. The diameter, length, thickness, and texture of the nanotubes can be further controlled with the template structure, number of infiltration, pristine particle size, and heat-treating temperature. The tubular SnO_2 (i.e., organized nanocrystallites) shows a significant improvement of electrochemical performance (a combination of a better cycle life and higher storage capacity) over the unorganized nanoparticles. The specific capacity of Sn-based nanotube electrode was 525 mAh/g after 80 cycles. In principle, as demonstrated in this work, the tubular structure of active component can also be extended to other Li−metal alloy systems. In view of their unique features, furthermore, the prepared SnO_2 nanotubes may also find interesting applications in other fields such as gas sensing.

Acknowledgment. The authors gratefully thank the Ministry of Education, Singapore, and the Singapore−MIT Alliance for financial support of this research.

Supporting Information Available: FESEM images of SnO_2 nanotubes, SEM images of the SnO_2 suspension after various infiltration cycles, and TEM images of the nanotubes taken from a Sn-based electrode. This material is available free of charge via the Internet at http://pubs.acs.org.

CM050724F

(33) Dominko, R.; Arèon, D.; Mrzel, A.; Zorko, A.; Cevc, P.; Venturini, P.; Gaberscek, M.; Remskar, M.; Mihailovic, D. *Adv. Mater*. **2002**, *14*, 1531.
(34) Chen, J.; Tao, Z. L.; Li, S. L. *Angew. Chem., Int. Ed.* **2003**, *42*, 2147.
(35) Li, N. C.; Martin, C. R. *J. Electrochem. Soc.* **2001**, *148*, A164.